ARMA e-NEWSLETTER
SPRING 2015

In this issue

SPECIAL ISSUE: Imaging and Remote Sensing in Rock Mechanics

Early in 2014, the ARMA Publications Committee undertook a new initiative: using Special Issues of the ARMA e-Newsletter as a platform for publishing technical notes on specific topics of wide interest to the membership. The first Special Issue on "Geomechanics of Hydraulic Fracturing in Shale Formations" (May, 2014) was received with great enthusiasm. Encouraged by the positive feedback, we are publishing a second Special Issue of the e-Newsletter; this time on the theme of "Imaging and Remote Sensing in Rock Mechanics."

With their non-destructive and non-contact nature, imaging and remote sensing techniques have unique advantages in helping us better understand rock deformation and failure mechanisms on the laboratory scale as well as on the field scale. In this special issue, we include four contributions. Kos and Amman illustrate the use of a portable radar interferometer for a case study monitoring rock block stability. Lin and Labuz discuss the applications of speckle methods, such as electronic speckle pattern interferometry (ESPI), and digital image correlation (DIC), in laboratory experiments. Kasperczyk *et al.* present a grid-based optical method for measuring fracture extension and opening in a hydraulic fracturing experiment. Finally, Benton *et al.* describe the use of photogrammetry for monitoring underground mining environments.

We hope that this special issue would stimulate your interest in these novel techniques for both research and practice in rock mechanics and rock engineering.

Please feel free to send us comments and suggestions regarding this issue, and Special Issues of the ARMA e-Newsletter in general. Suggestions of new topics for future Special Issues are also welcome.

Address your comments to: **bhaimson@wisc.edu**

Haiying Huang.

On behalf of ARMA Publications Committee

Invitation to San Francisco

The American Rock Mechanics Association invites you to its 49th US Rock Mechanics/Geomechanics Symposium, to be held in San Francisco, California, USA on 28 June-1 July 2015. The 2015 program will focus on new and exciting advances in rock mechanics and geomechanics. San Francisco is one of the country's most dynamic cities. Home to some of the world's most innovative companies (Silicon Valley is nearby), San Francisco is known for its beautiful hills and views, its world-class restaurants, and its sophisticated cultural institutions. The symposium will be held at the Westin St. Francis on Union Square in the heart of the city. This year, ARMA is pleased to offer childcare services for participants who may want to bring families to enjoy San Francisco.

Papers, Posters, and Other Features

The symposium technical committee selected 366 papers from over 650 abstracts. Forty-eight technical sessions are planned over three full days. The sessions will feature rock mechanics and geomechanics presentations on petroleum engineering, mining engineering, civil engineering and interdisciplinary topics. Presentations will include posters and podium deliveries. The popular ARMA Trivial Pursuit competition will take place, along with the Career Center display for employment opportunities.

Two short courses are offered: Rock Fracture Process Modeling Using FDEM, and InSAR and Its Application to Mining. Three one-day workshops are included: Workshop on Geomechanics in Unconventionals for Industry Professionals: From Characterization to Production; Workshop on Digital Rock Physics Derived Rock Mechanics Properties; and Workshop on How to Give an Effective and Engaging Presentation.

Three technical tours are scheduled: Faulting in San Francisco Bay Area Tour; San Francisco Bay Geological Engineering Tour with Dick Goodman; and the Geysers/Napa Valley Technical Tour. Special events include major league baseball, various city landmarks, social activities and other attractions.

Keynote Speakers

The Symposium will feature a lineup of provocative and interesting speakers for keynote addresses. The list will include:

• James R. Rice, Mallinckrodt Professor of Engineering Sciences and Geophysics, Harvard University, will lead off with the MTS Lecture on the topic: "Thermo-Poro-Mechanics of Shear Localization in Rapidly Sheared Granular Rock."

• Kate Hadley Baker, Retired, BP and ExxonMobil, on "Some Thoughts on Rock Mechanics in the Oil and Gas Industry."

• Christopher Mark, Principal Roof Control Specialist, Mine Safety and Health Administration on "The Science of Empirical Design in Mining Rock Mechanics."

• Steven Glaser, Department of Civil and Environmental Engineering, University of California, on "Friction Mechanics, Onset of Sliding, and Laboratory Quakes."

Join us. For more information or early registration, use website www.armasymposium.org

Characterizing Rock Slope Deformations With a Portable Radar Interferometer

ByAndrew Kos, Terrasense Switzerland Ltd, (Werdenberg, Switzerland)/Institute for Geotechnical Engineering, ETH (Zurich, Switzerland), and Florian Amman, Geological Institute, (ETH Zurich, Switzerland)

Introduction

Terrestrial radar interferometry (TRI) uses phase coherent, imaging radar technology and interferometric methods for measuring spatial deformations at high precision for geological and geotechnical applications. The general technique involves the use of radar sensors that actively emit a phase coherent signal in the form of a microwave beam using a real aperture antenna. A number of different radar imaging techniques are used for terrestrial radar interferometry. These include the use of dish-shaped (Reeves et al 2001), synthetic aperture (Leva et al 2003) and slotted waveguide antennae (Werner et al 2012). Regardless of the imaging technique, the emission of a phase coherent signal is a prerequisite for determining changes in differential phase, and hence the measurement of deformation. The basic principle of interferometry involves the subtraction of phase from one radar image to another. (For further details concerning terrestrial interferometric methods, the reader is referred to Caduff et al (2015)).

In this contribution, we outline a case study of an unstable rock block where deformations were imaged using an innovative, real aperture portable radar interferometer. The presented case study demonstrates the utility of high resolution imaging of spatial deformations, which support the characterization of rock slope behavior and failure mechanisms.

Portable radar interferometry

The portable radar interferometer used in this study is a Ku-band (17.2 GHz) real aperture FMCW system consisting of one transmitting and two receiving antennae (Figure 1) (Werner et al 2012). Movement is measured along the radar line of sight (LOS), with a measured precision as low as 0.2 mm (Caduff et al 2014). At ranges greater than ~1,000 meters atmospheric perturbations may affect the data quality, however a range of data processing strategies may be employed requiring specialized knowledge to reveal the characteristics of the radar signals representing rock slope deformation.

Radar images are acquired by rotating the antennae around a central axis. The field of view is programmable to 360 degrees and rotation velocity is 10 degree/sec. In practical terms, rapid scene acquisition allows for (1) highly coherent radar images with high data quality, (2) coherent tracking of fast moving objects (e.g. ~0.3 mm/sec), relevant for near real-time monitoring involving critical failure, and (3) stacking many images to reduce atmospheric effects.

Figure 1. Examples of a portable radar interferometer mounted on a heavy-duty survey tripod (left) and on a simple 18 x 18 cm stainless steel plate (right).

Case study: Rock block instability

The study site is large rock wall consisting of Gneiss (H ~300 m, L ~600 m), which has been the scene of several block failures in recent years, the largest of which occurred in 2007 (~3,000 m^3) followed by two smaller events in 2008 and 2009 (< 500 m^3) (Kos et al 2011). A large unstable block undergoing progressive failure (~3,000 m^3) remains partially attached to the rock wall. In 2013, an earth dam was constructed by the roads authority to protect the adjacent state roadway from future block falls.

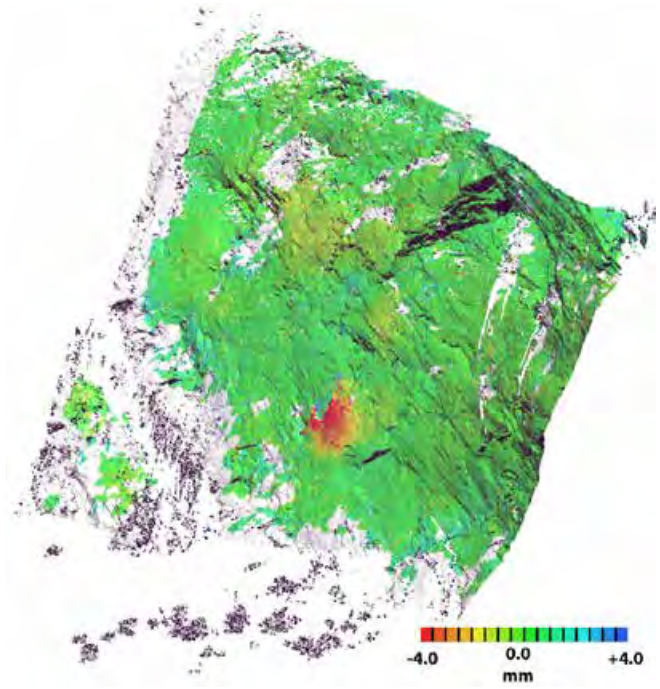

Figure 2. Radar interferometric deformation map projected into a high resolution 3D point cloud from laser scanning. The magnitude of deformation is 4.0 mm within a 3 month period. View is toward the southeast, deformations in the negative direction are towards the radar instrument.

Radar interferometric measurements were undertaken as part of research project into rock fall release mechanisms. The radar instrument was mounted on a heavy duty survey tripod, which was levelled and centered with respect to a fixed reference point. A total of 7 campaigns lasting 3-4 hours were acquired between March 2010 and November 2011. The distance between the radar and the measured object was ~600 meters.

An interferometric deformation map is shown in Figure 2, derived from three measurement campaigns undertaken over a three month period. The deformation map has been projected into a high resolution three-dimensional point cloud from laser scanning (Figure 2) and a high resolution photogrammetric model (Figure 3). The technique allows a precise delineation of observed deformation with respect to geological structures and lithological boundaries.

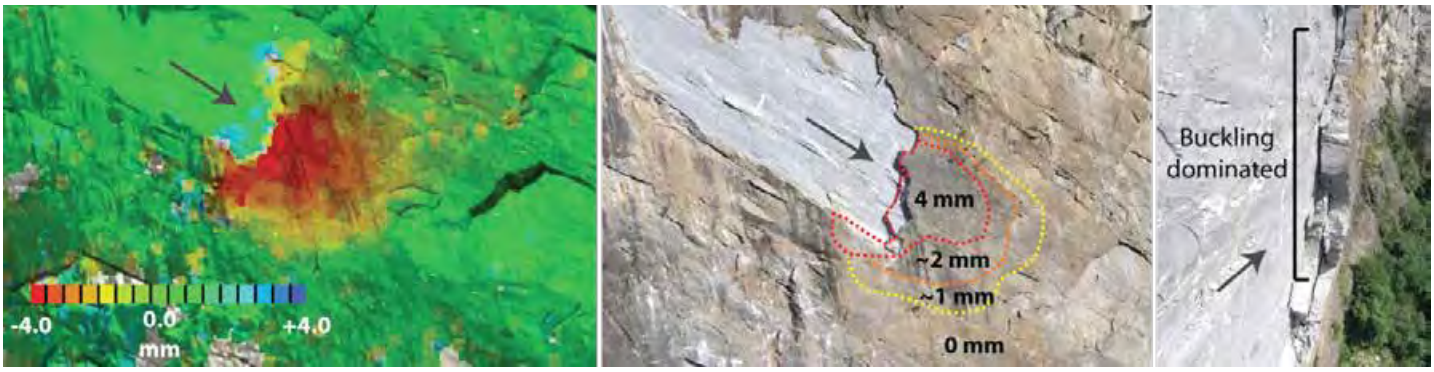

Figure 3. Detail of the radar interferometric deformation signal projected into a high resolution photogrammetric 3D model (left), contoured deformation field of the unstable rock block (center) and side-looking view of the unstable rock block showing a buckling mechanism (right)

Detail of the radar interferometric deformation signal is shown in Figure 3. The deformation field is characterized by more intense movement to the left of the block, which gradually diminishes in both the horizontal and vertical directions. This pattern indicates a dominant buckling failure mechanism, which is also evident from field observations (Figure 3). Crackmeters installed at three locations along the left margin of the rock block corroborate the magnitude of deformation observed in the radar data. Several environmental parameters are also being monitored (e.g. rainfall, shallow rock and ambient air temperature)

For most instabilities with low deformation rates, the portable radar interferometer can be utilized for tracking movements through the implementation of periodic measurement campaigns. An example of this is shown in Figure 4 where measurements undertaken at periodic intervals between 2010 and 2011 showed preliminary evidence of seasonal effects, influencing deformation. In this case, slightly elevated deformations are observed to take place prior to and during the autumn months when ambient atmospheric temperatures begin to progressively cool.

Conclusions

The case study presented results of radar interferometric measurements of an unstable rock block using a portable radar interferometer. The high spatial resolution of the radar results combined with laser scanning and photogrammetric-based visualization enabled recognition of buckling as a dominant failure mechanism. Periodic measurements over ~2 years indicated seasonal influences on the temporal deformation field. The results from the portable radar interferometer demonstrate the utility of the technique and method for geological and geotechnical investigations and monitoring.

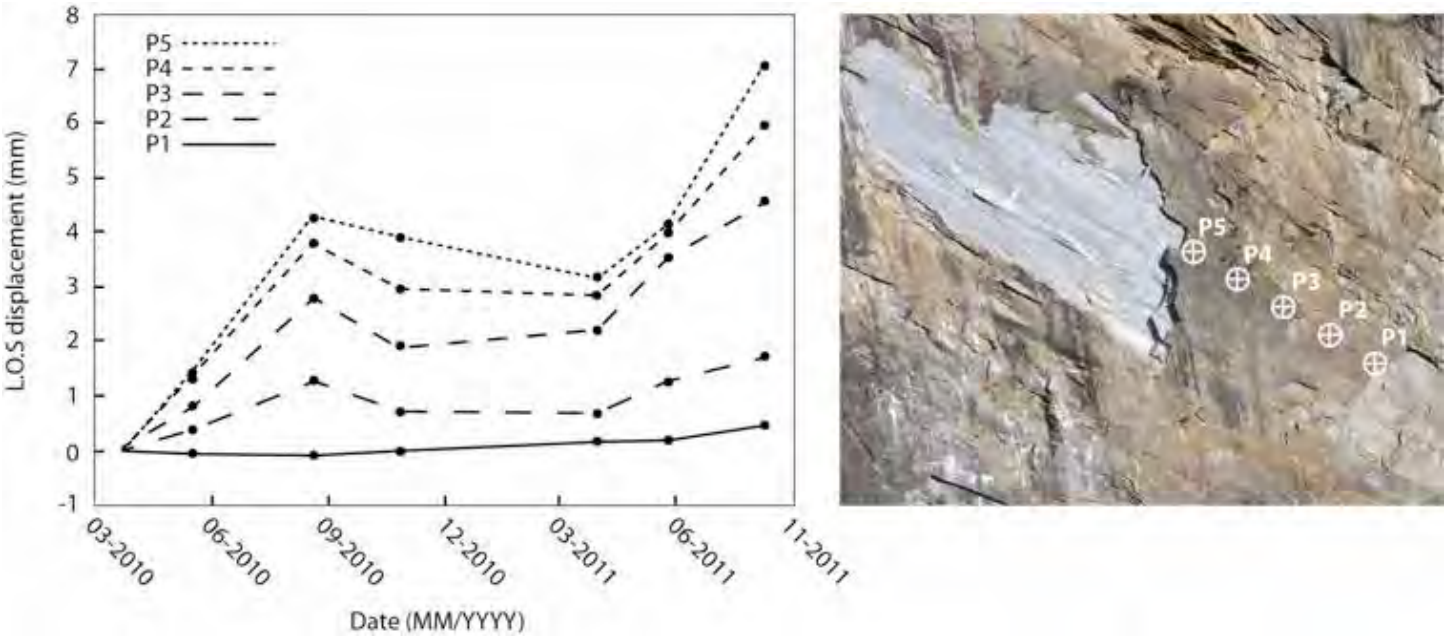

Figure 4. Radar interferometric deformation measurements showing possible evidence of seasonal influences (left). P1-5 are points selected in the radar interferometric deformation maps (right).

References

Caduff, R. Kos, A., Schlunnegger, F., McArdell, B. & Wiesmann, A. (2014) Terrestrial radar interferometric measurement of Hillslope Deformation and Atmospheric Disturbances in the Illgraben Debris Flow Catchment in the Swiss Alps. IEEE Geoscience and Remote Sensing Letters. Vol. 2, No.11.

Caduff, R. Schlunnegger, F., Kos, A., & Wiesmann, A. (2015) A review of terrestrial radar interferometry for measuring surface change in the geosciences. Earth Surface Processes and Landforms Vol.40, 208-228 DOI: 10.1002/esp 3656.

Kos, A., Strozzi, T., Stockmann, R., Wiesmann, A. & Werner, C. (2011) Detection and characterization of rock slope instabilities using a potable radar interferometer. Proceedings Second World Landslide Forum, Oct 3-7, Rome.

Leva, D., Nico, G., Tarchi, D., Fortuny-Guasch, J. & Sieber, A. (2003) Temporal analysis of a landslide by means of a ground-based SAR Interferometer. IEEE Transactions on Geoscience and Remote Sensing 41: 745-752. DOI:10.1109/TGRS.2003.808902

Reeves, B., Noon, D.A., Stickley, G.F. & Longstaff, D. (2001) Slope stability radar for monitoring mine walls. Proceedings of SPIE, 57-67. DOI:10.1117/12.450188.

Werner, C., Wiesmann, A., Strozzi, T., Kos, A. & Caduff, R. (2012) The GPRI multi-mode differential interferometric radar for ground-based observations. Proceedings, 9th European Conference on Synthetic Aperture Radar; 304-307.

News Briefs

ARMA Board of Directors. In the recent election, the following members were elected to serve on the Board of Directors: Loren Lorig, Joe Labuz, Maria-Katerina Nikolinakou, and Joe Morris. Further, Derek Elsworth was appointed to replace Rico Ramos for the remainder of his term (June, 2017). In addition, the new officers are John McLennan (President), Laura Pyrak-Nolte (Vice-President), John Curran (Treasurer), and Kate Baker (Secretary).

National Academy of Engineering appointment. Derek Elsworth, ARMA Fellow and a member of the Board of Directors, was honored by election to NAE in February. He is professor of energy and geo-environmental engineering at Pennsylvania State University (University Park). He was cited for his contributions to understanding natural processes affecting flow and transport properties of fractured rocks.

Speckle Methods and Their Applications

By Qing Lin, College of Petroleum Engineering, China University of Petroleum, Beijing, and Joseph F Labuz, Department of Civil, Environmental, and Geo- Engineering, University of Minnesota.

Introduction

Speckle methods use a random speckle pattern (Fig. 1) generated by surface structure, naturally or artificially, as a carrier to extract information on displacements, and with processing, strains. In this article, two main speckle methods, electronic speckle pattern interferometry (ESPI) and digital image correlation (DIC), are explained, and principles, system calibration, and applications to rock mechanics are discussed.

Principles of ESPI and DIC

• Electronic speckle pattern interferometry (ESPI)

Surface structure for most materials is rough enough to generate scattering of light, such that a speckle pattern is created (Fig. 1a). The dark and bright spots are the consequences of a large number of superpositions from scattered light waves. The irradiance changes of speckles can be used to obtain information about surface displacements on the scale of the light wavelength (Butter and Leendertz 1971, Macovski et al. 1971). A typical setup of an ESPI system is a double laser beam interferometer (Haggerty et al. 2010). It measures uni-directional displacement (e.g. x-direction) because the optical configuration eliminates the influence of the other in-plane displacement as well as the out-of-plane displacement. Thus, the *x*-direction displacement u_x can be determined by EPSI:

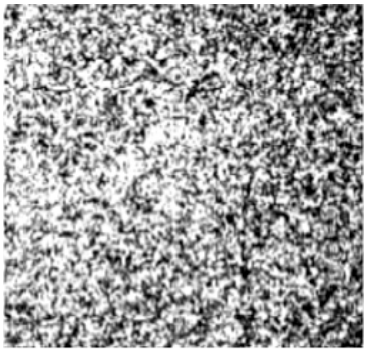

Figure 1 (a): Random speckle patterns, optical speckles from ESPI

$$u_x = \frac{n\lambda}{2\sin\Theta} \qquad (1)$$

where n is the fringe number, λ is the wavelength, and Θ is the angle between the incident beam of light and the normal of the specimen surface.

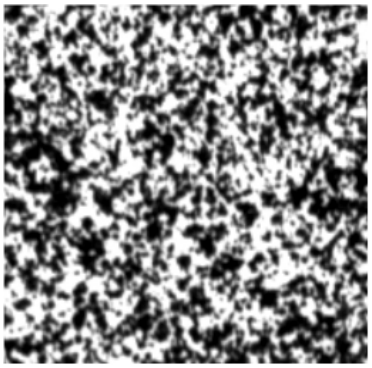

Figure 1 (b): Random speckle patterns, painted speckles from DIC.

• Digital image correlation (DIC)

ESPI decodes the phase information in the speckles to produce fringes based on the optics; in contrast, DIC is conceptually simple since this technique traces a unique feature on the specimen surface to obtain displacements (Chu et al 1985; Sutton et al 2009). For example, a speckle painted on the surface (Fig. 1b) can serve as a target to determine its movement between two images. However, the irregularity of a speckle makes it almost impossible for a computer algorithm to identify. Thus, a grid ($m \times m$ pixels) called a subset, which contains several speckles with a unique intensity pattern, is selected as the target, and a relatively larger area ($n \times n$ pixels) called the region of interest (ROI) is selected as the searching area. The degree of similarity between the original and deformed subsets can be evaluated by a cross-correlation algorithm, where the peak position of cross-correlation values represents the displaced position of the subset. The cross-correlation function (*CC*) is defined as the two-dimensional spatial convolution of *I* and *I**:

$$CC = \sum_{i=1}^{m}\sum_{j=1}^{m} I(x_i, y_j) I^*(x_i^*, y_j^*) \qquad (2)$$

where I and I* are intensity values from the reference and current images respectively. For a given subset, there exists a maximum value of the cross-correlation function in the ROI, where it satisfies the conditions $x^* = x + u_x$ and $y^* = y + u_y$, and thus it is possible to determine the displacement of the subset (u_x, u_y). Note that DIC measurements involve the influence of a magnification factor *M*, because the DIC algorithm gives the results of displacements in pixels. For a known magnification factor *M*, the actual displacements can be computed (Lin and Labuz 2013).

It should be noted that the two speckle patterns in Fig.1 are completely different, even though they look similar. The pattern in Fig. 1a is generated by an interference effect of the specimen surface, while the pattern in Fig. 1b is created artificially by coating or painting the specimen surface. In addition, pattern (a) is superimposed on the specimen surface, and more importantly, it may "decorrelate" if the displacement is large; pattern (b) is glued on the surface and it moves with the specimen, since only perfect adherence of the coating material is considered.

System calibration

• Rigid body translation

The simplest displacement field is rigid body translation. A block of material (Berea sandstone) was translated over a known distance using a

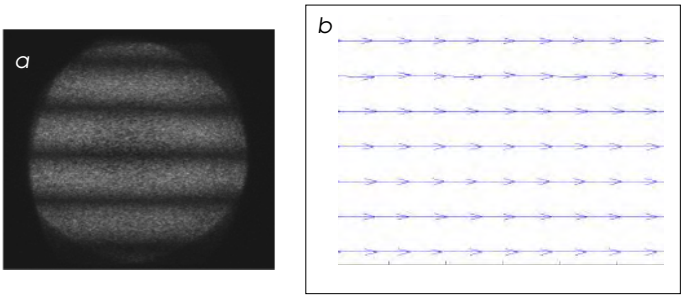

Figure 2: Experimental results from rigid body translation, (a) ESPI fringe pattern (b) DIC measured displacement field

Vernier scale with 2 μm resolution. The ESPI measurements resulted in a series of parallel horizontal fringes (Fig. 2a), indicating that there is no displacement gradient across the field of view in the horizontal direction. The spacing between parallel fringes is associated with the ESPI system and the amount of translation. A relation can be established between the fringe spacing and the translation value, and system error can be estimated.

The DIC measurements give a set of displacements with respect to the total number and distribution of subsets (Fig. 2b). Since the individual displacement may vary, the average value of the displacements is taken as the measured DIC value. The system accuracy can be determined by comparing the measured DIC value to the induced displacements

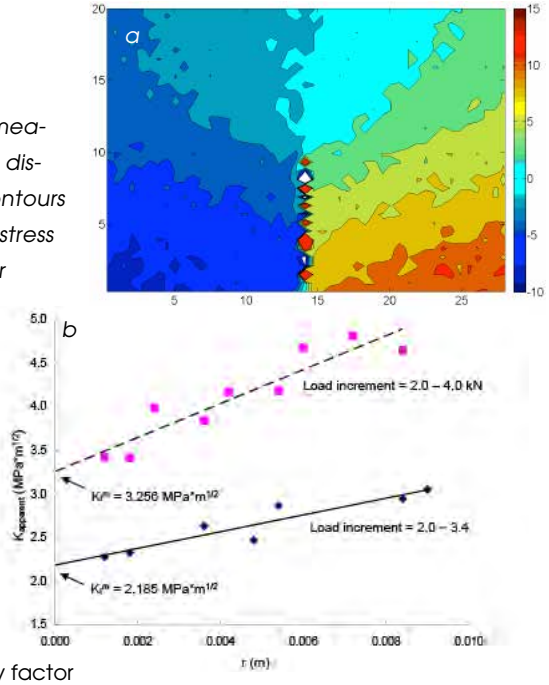

Figure 3: DIC measurements, (a) displacement contours (b) estimated stress intensity factor

- Stress intensity factor

The crack opening displacement (COD) near the crack tip is related to the model stress intensity factor (K_I) through the classic relationship from linear fracture mechanics. Thus, the information of COD that is extracted from the horizontal displacements measured by DIC (Fig. 3a) can be used to compute a measured K_I^m. Depending on the distance from the crack tip, an apparent K_{app} can be calculated based on DIC measurements, and K_I^m is the *y*-intercept of a best fit line through the data of K_{app}. Fig. 3a illustrates the DIC measurements as contours of displacement for the load increment of 2.0 – 3.4 kN for a three-point bend test on an aluminum beam. The results of the fracture analysis are shown in Fig. 3b, with the measured K_I^m = 2.185 MPa*m$^{1/2}$ and the theoretical K_I^t = 2.253 MPa*m$^{1/2}$, a difference of 3%. Fig. 3b also shows the results for the load increment of 2.0 – 4.0 kN, showing a difference between the measured and theoretical value of 1%.

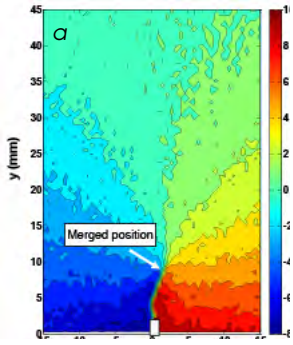

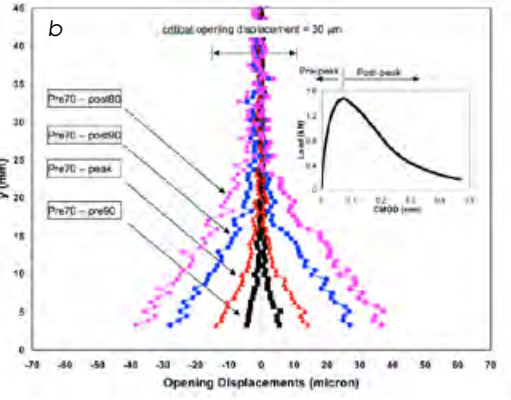

Figure 4: DIC measurements, (a) displacement contours (b) opening displacements along the fracture.

Application to rock mechanics

One application of speckle methods is to identify fracture initiation (and propagation) under different loading conditions (Lin et al. 2009, 2014). As an example, a Berea sandstone beam was loaded to failure in a three-point bend test. Fracture initiation is revealed by the displacement contours determined from DIC. As shown in Fig. 4a, the region between the merged position of the displacements and the notch tip clearly displays a discontinuity in displacement. Fig. 4b gives the opening displacements along the fracture at various loading stages. Thus, speckle methods provide high-resolution information on displacements (and related strains).

References

Butters JN, Leendertz JA. Holographic and video techniques applied to engineering measurements. J Meas Control 1971, 4, 349-354.

Chu TC, Ranson WF, Sutton MA, Peters WH. Applications of digital-image-correlation techniques to experimental mechanics. Exp Mech 1985; 232-244.

Haggerty M, Lin Q, Labuz JF. Observing deformation and fracture of rock with speckle pattern. Rock Mech Rock Eng 2010, 43(4): 417–426.

Lin Q, Fakhimi A, Haggerty M, Labuz JF. Initiation of tensile and mixed-mode fracture in sandstone. Int J Rock Mech Min Sci 2009, 46: 489-497.

Lin Q, Labuz JF. Fracture of sandstone characterized by digital image correlation. Int J Rock Mech Min Sci 2013, 60: 235-245.

Lin, Q, Yuan H, Biolzi L, Labuz JF. Opening and mixed-mode fracture processes in a quasi-brittle material via digital imaging. Eng Fract Mech 2014, 131: 176-193.

Macovski A, Ramsey SD, Scheafer LF. Time-lapse interferometry and contouring using television system. Appl Opt 1971, 10: 2722-2727.

Sutton MA, Orteu J, Schreier HW. Image correlation for shape motion and deformation measurements. New York: Springer; 2009.

Experimental Two-Dimensional Hydraulic Fracture Growth and Opening Measured Using a Grid-Based Optical Method

By D. Kasperczyk, R.G. Jeffrey, and J. Kear, Commonwealth Scientific and Industrial Research Organization (CSIRO), Melbourne, Australia

Introduction

Continuous displacement often needs to be measured during laboratory rock fracture experiments. Popular techniques for optically measuring sample displacement and strain include speckled digital image correlation (DIC) and moiré interference patterns. However, there are occasions when the experimental set up is not conducive to using these techniques because of limited space or unfavourable light conditions.

The grid measurement method described here uses a digital camera to measure movement of a grid drawn on a rock surface to 10x better than pixel resolution. The grid measurement method is simple and effective and includes advantages similar to other remote sensing imaging methods such as non-contact measurement, real-time continuous measurement, and sub-pixel resolution. Unlike some other imaging methods, it is easy to correct image distortion, can be used in poorly lit space-constrained experimental setups, and in instances where the camera position may move relative to the sample during testing.

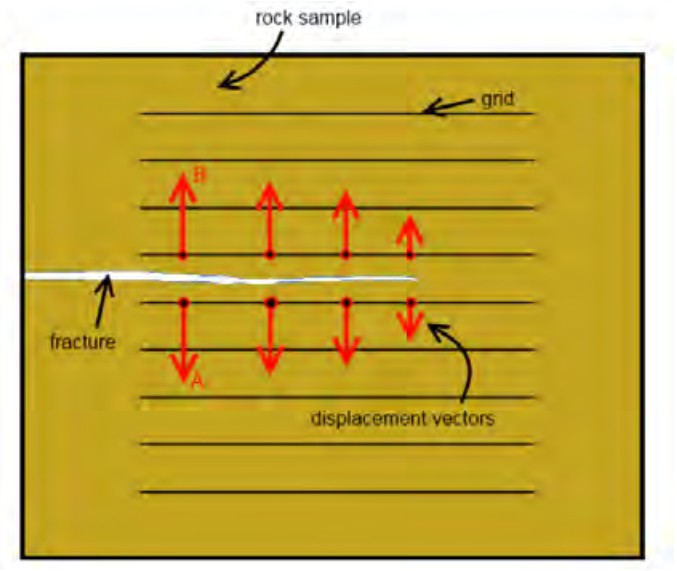

Figure 1 – Rock sample with grid parallel to the fracture plane. Fracture opening is equal to the differential displacement of the gridlines on either side of the fracture.

The method was developed for measuring fracture opening of two-dimensional hydraulic fractures in rock samples confined in a true triaxial load frame (Jeffrey et al., 2015). This experimental apparatus is designed to allow for both recording of the fracture path and measurement of fracture opening. The hydraulic fracture path is controlled by applied stresses and opening occurs perpendicular to the fracture path. Considering the fracture opens perpendicular to the grid, fracture opening can be calculated by measuring differential movement of the grid on opposing side of the fracture path in a single plane (Figure 1).

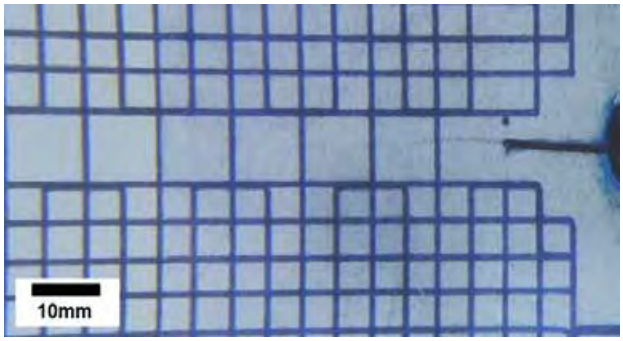

Figure 2 – Gridlines in 5 x 5 mm grid printed on a rock sample. The horizontal fracture path can be seen originating from a 1mm thick notch extending about 12mm on the right side of the image.

Method

In experiments such as presented in Jeffrey et al. (2015), a hydraulic fracture is grown horizontally from the centre of a 350 x 350 x 50 mm siltstone sample. A 5 mm square grid is printed onto the rock sample using a plotter, although a 10 mm square grid is used in areas where an unobstructed view is needed (Figure 2).

A digital camera is used to record a video of the grid at 25 frames per second with a resolution of 1920 x 1080 pixels. The resultant pixel size for the described case is 80 x 80 µm. The grid is used to provide a known square coordinate reference to correct for any image keystone and barrel distortion.

To measure fracture opening, the relative movement of the centre of each gridline is analyzed. After removing all image distortion, the video footage is processed by a correlation algorithm to locate each gridline. The set of pixels across each gridline are then fitted with a Gaussian distribution and subsequently a least-squares fit to calculate the centre of each gridline.

At any location along the fracture path, the fracture opening is measured by the differential displacement of two gridlines on opposing sides of the fracture path (labels A and B in Figure 1). Elastic deformation of the rock between the gridlines causes the opening to be underestimated when measured this way, but this error is small for the experimental configuration used here.

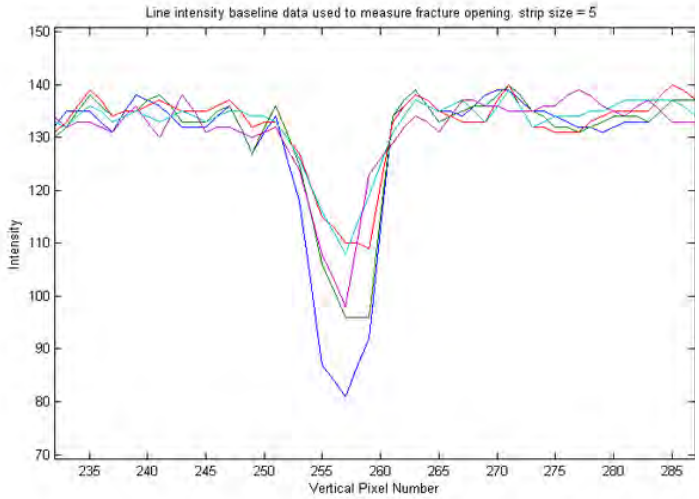

Figure 3 – Pixel intensity data along a gridline. The five colored series shown represent the selected location and four adjacent pixel strips to the selected location. The data are for one frame only.

Two averaging variables, strip size and image stack, are used to reduce noise and increase measurement accuracy (Pan et al., 2009). Strip size includes pixels adjacent to the target location to optically dither the results. A line intensity chart with strip size of 5 pixels (0.42mm) is shown in Figure 3 where each colored line represents pixel intensity values adjacent to the target location. Increasing the strip size parameter increases the precision of the gridline center location. However if an overly wide strip is analyzed an error is introduced, since the magnitude of the fracture opening is not uniform through the grid.

The image stack variable averages the intensity values of analyzed pixels over a set time period. By using a half-second time period, assuming 25 frames per second are captured, 12 images are stacked together to make two discrete measurements per second. The image stack technique reduces noise and increases measurement accuracy; however, increasing the image stack exaggerates small errors as the fracture opening varies with time.

In order to validate the presented grid measurement method, a test bed was created to provide calibration displacement measurements. This test bed allowed comparison of data from two optical methods (grid measurement and speckled DIC) to direct measurements of displacement from a Linear Variable Displacement Transducer (LVDT).

The test bed displaced a sample marked with a 5 x 5 mm grid and a speckle DIC pattern at 0.4µm per second while recording images at 25 frames per second at a resolution of 1920 x 1080 pixels. In this test bed example, one pixel represented an area of 180µm x 180µm.

Results

Optical data from the test bed calibration experiments have been

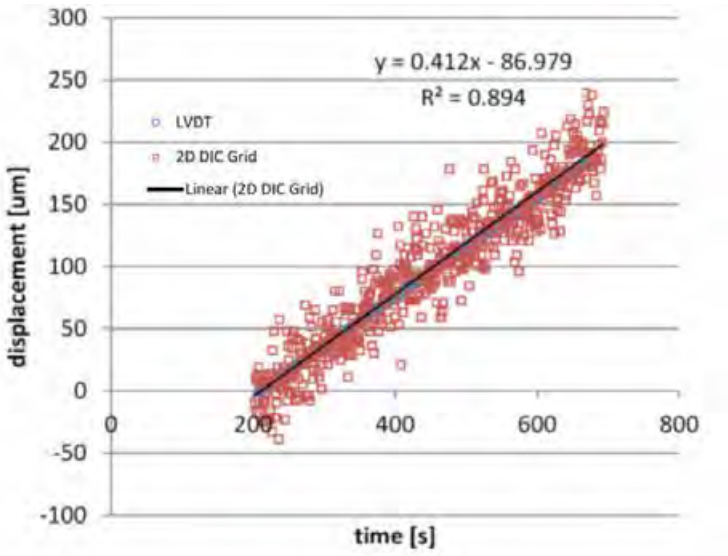

Figure 4 – Grid displacement (red) without averaging variables.

analyzed with and without the use of the two averaging variable techniques (strip size and image stack). Without using the averaging variables techniques, the long-term linear correlation of the optical measurements provides a close match to the direct LVDT measurement. However, the instantaneous optical measurement results give a poor match to the direct LVDT measurements with an instantaneous error of around 80 µm (Figure 4).

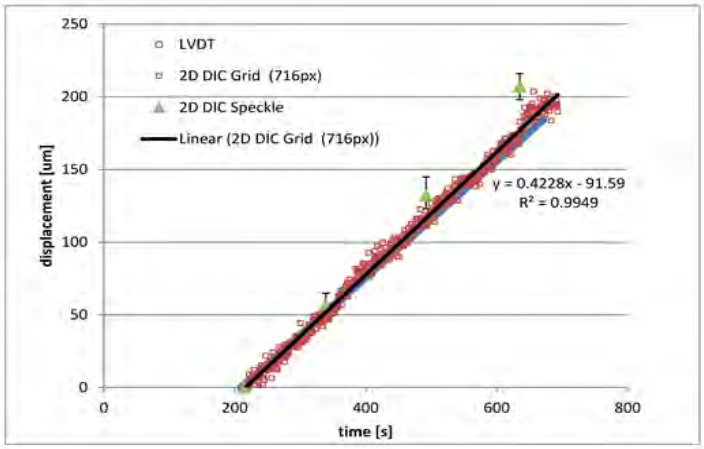

Figure 5 – Grid-displacement method (red) compared to DIC speckle (green), and to LVDT (blue)

When analysing the same data using the two averaging variable techniques (strip-size = 5, image stack = 12), a good long-term match to the LVDT data and much smaller instantaneous measurement error of ~ 8 µm was obtained (Figure 5).

Displacement and strain were also calculated with images of a 2D DIC speckle pattern using Ncorr software (Blaber et al., 2015). The long-term match to the LVDT data gives a 20% error and the instantaneous error was ~ 30 µm (Figure 5). All of the above results are summarized on the following table. This error is not indicative of the quality of the Ncorr software package, merely its accuracy in this specific experimental setup.

Method	µm per second	Coefficient of determination (R-squared)	Measurement Error
LVDT	0.401	1.000	< 1 µm
Grid without averaging variables	0.412	0.894	~ 80 µm
Grid with averaging variables	0.423	0.995	~ 8 µm
2D speckle	0.485	n/a	~ 30 µm

Concluding Remarks

The presented grid measurement provides a simple and easy method to optically measure sample displacement for cases where the displacement is perpendicular to applied gridlines. The presented calibration case demonstrates that the grid measurement method is capable of providing accurate and precise displacement results through the analysis of grid deformations. The suitability of the grid measurement method is however dependent on experimental conditions. If the fracture curves significantly away from the grid direction, the averaging calculation must be corrected for the change in relative orientation between the gridline and fracture. A similar problem can arise for opening measurements near the fracture tip where the opening displacement is small and can be lost in the noise; also, averaging pixels near the tip may degrade the measurement since the opening displacement is changing rapidly with position.

Nevertheless, the method described here provides a simple approach that can be used to measure displacement to a resolution at least 10 times better than pixel size.

References

Blaber, J., Adair, B., & Antoniou, A. (2015). Ncorr: Open-Source 2D Digital Image Correlation Matlab Software. Experimental Mechanics, 1-18.

Jeffrey, R. G., Kear, J., Kasperczyk, D., and Zhang, X. (2015). A 2D experimental method with results for hydraulic fracture crossing discontinuities. In 49th North American Rock Mechanics Symposium. American Rock Mechanics Association.

Pan, B., Qian, K., Xie, H., & Asundi, A. (2009). Two-dimensional digital image correlation for in-plane displacement and strain measurement: a review. Measurement science and technology, 20(6), 062001

News Briefs

Engineering Mechanics Institute (EMI) award. The American Society of Civil Engineering (ASCE), through its affiliate EMI, will present its Maurice A. Biot Medal to Emmanuel Detournay (Ph.d, University of Minnesota). The award cites him "for contributions to the application of Biot's theory of poromechanics to rocks, and specifically for the lasting impact of Dr. Detournay's scholarship on hydraulic fracturing modeling and monitoring in both academia and industry." The presentation will take place at the EMI 2015 Conference at Stanford University, 16-19 June, 2015.

Using Photogrammetry to Monitor Underground Mining Environments

By D. Benton. M. Boltz, M Raffaldi, and S. Iverson, National Institute for Occupational Safety and Health, (NIOSH) Spokane, Washington.

Abstract

Photogrammetric methods are advancing rapidly and show considerable promise as a ground control research and monitoring tool. The ability to quickly capture three-dimensional geometry in field and laboratory settings is a significant advancement in deformation monitoring. Photogrammetry is being applied in both settings as part of the NIOSH ground control research program. This paper describes three applications of photogrammetry for use in ground control monitoring. First, photogrammetry was used to measure complete patterns of ramp rib and back deformation caused by creep and mining-induced seismicity. The results of this application are being used in a mine visualization project. Second, relative displacements across seismically active faults were measured photogrammetrically. Case studies are provided that illustrate how photogrammetry may be used to supplement crackmeter monitoring systems. Third, photogrammetry was used in laboratory tests to delineate the relationship between shotcrete and mesh intra-bolt bulge deformation and residual support strength. Results of this application were applied to field situations.

Introduction

Photogrammetry systems were implemented by researchers at the National Institute for Occupational Safety and Health (NIOSH) Spokane Mining Research Division (SMRD) as part of its ground control research to improve mine safety. Data collection may take as little as a few minutes, can be performed at safe distances from hazardous ground conditions, and can capture complete geometry for laboratory analysis. NIOSH/SMRD researchers have demonstrated that photogrammetry can produce millimeter-level measurements in three different applications. First, photogrammetry has been used to measure three-dimensional patterns of excavation deformation. The results of this application are being used to document temporal changes in ground conditions. Second, ground displacement across seismically active faults was measured photogrammetrically. Case studies have shown that photogrammetry can successfully separate global from local ground movements, thus more clearly describing fault behavior. Third, photogrammetry was used in laboratory tests to establish relationships between support system deformation and residual support strength. A series of volume-energy relationships for different support systems is being completed for industry use in assessing support performance. All three applications of photogrammetry will improve analysis and response to changing ground conditions, and in turn, increase worker safety.

The photogrammetry system software, hardware, and methodology were previously explained by Benton, et al. (2014, 2015). A photogrammetry system produced measurement accuracies within 1.0 mm in laboratory conditions (Benton, et al., 2014). In field settings, this system had an average accuracy of 8.0 mm when compared to crackmeter measurements (Benton, et al., 2015). A separate laboratory system had a linear accuracy of 2.0 mm, and a volumetric accuracy of 1.8% (Benton, et al., 2014). This system was used to monitor high energy, high deformation testing of shotcrete panel and mesh support systems (Martin, et al., 2015).

Excavation Profile Monitoring

Photogrammetry was used by NIOSH/SMRD researchers to monitor fault exposures at a deep underground mine. Quarterly photogrammetric surveys of three separate fault structures at the participating mine were conducted, beginning in January 2013. The mine in this study has three faults intersected by a ramp system at nine locations, spanning seven levels, with no more than one fault structure at each site. Using photogrammetric data from these sites, cross-sections of the fault exposures can be represented via points and coordinates. If these cross-sectional profiles are compared over time, geometric changes to the ramp can not only be visualized, but measured using the point cloud data. The cross-sections may be developed at any location and at any orientation to allow for total site analysis.

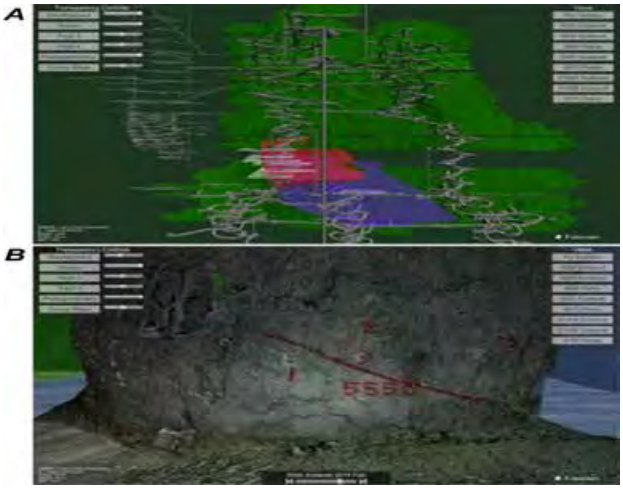

Figure 1. Screen captures from the Unity visualization tool showing (A) an overview of the workings and (B) a photogrammetric reconstruction in the visualization tool. The blue and red in (A) represent faults.

A visualization tool was created that allows the user to interact with a 3D visual model of the participating mine, which integrates and visualizes the results of excavation profile monitoring (Orr et al., 2015). The visualization tool was created using Unity® (Unity Technologies, 2015), which is a development platform for designing video games and other interactive programs. The visualization tool consists of a model of the mine workings, seen in Figure 1A, that the user can navigate in order to view the workings and geologic features of the mine. The user also has the option to enter the workings in specific areas of the mine

to view the photogrammetric reconstructions (Figure 1B), scrolling through each sequentially to see how the site is changing. To date, quarterly reconstructions can be viewed for nine different sites from January 2013 to January 2015. Work is also underway to integrate photogrammetric data with other research results such as the locations of recorded seismic events and geotechnical instrumentation data.

Fault Behavior Characterization

• *Crackmeter supplementation*

A second application of photogrammetry investigated by NIOSH/SMRD researchers provided supplementary data to the crackmeter measurements. The participating mine uses vibrating wire crackmeters to monitor fault movement. These crackmeters are designed specifically for monitoring movement across natural rock joints in the civil and mining industries. The instrument is placed across the joint of interest and anchored into the rock to measure ground movement. However, because crackmeters measure displacement in a single direction, the measurement is likely only a component of actual fault offset. Point cloud measurements provide a more complete picture of 3D movements, e.g., folding and squeezing deformation. Photogrammetry's ability to observe changes in crackmeter location and orientation over time can provide additional information about rock mass movement.

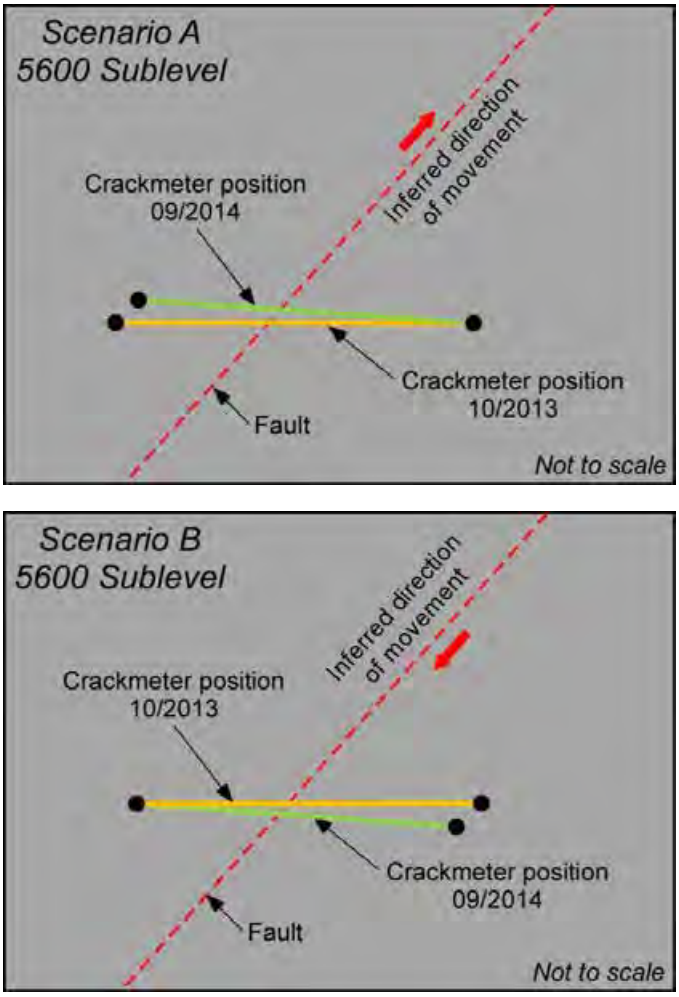

Figure 2. Representations of 5600 Sublevel analysis based on observed shortening of the crackmeter

• *Case study 1 – 5600 Sublevel*

Conditions at the 5600 Sublevel provided a good environment to test the capabilities of photogrammetric monitoring. Mine personnel observed severe stress-induced pillar deterioration that ultimately necessitated bypassing and backfilling the site (Board, 2015). Photogrammetric analysis was conducted to determine whether fault movement also influenced pillar deterioration.

Analysis of crackmeter data focuses on shortening and lengthening of the crackmeter. Depending on the orientation of the fault crossing the crackmeter, a sense of direction of fault motion can be ascertained. This technique is illustrated in Figure 2. In Scenario A, the initial crackmeter location (gold bar, October 2013) is oriented such that upward movement of the hangingwall would result in shortening of the crackmeter. The final crackmeter position (green bar, September 2014) represents the scene after movement has occurred. Alternatively, as shown in Scenario B, the footwall could have moved downwards, also resulting in a shortening of the crackmeter. In either scenario, the relative motion is the same, suggesting dip-slip offset of the fault.

However, analysis of the crackmeter data at the 5600 Sublevel cannot account for other observed deformations. The ~30 cm rib dilation observed by mine personnel indicates more significant movement than that registered by the crackmeter. In addition, photogrammetric survey data also indicated widespread movement, including rib convergence. To investigate this, global coordinates of each crackmeter anchor were used for a photogrammetric time lapse comparison between October 27, 2013 and September 28, 2014. During this period, the entire crackmeter was observed photogrammetrically to have moved an average of 24 cm outwards, and roughly 15.5 cm upwards.

Additional points on either side of the fault were selected for similar analysis. Global displacements for all these points were produced in mine global coordinates of easting, northing, and elevation (x, y, and z, respectively). To determine a comprehensive representation of the fault activity at the 5600 Sublevel site, the global x, y, and z displacements were transformed into local coordinate displacements oriented on strike and dip of the fault. Photogrammetric data indicated a strike of N 63° E, which served as the new y-axis. A fault dip of 58° was used for the second transformation, which served as the direction of the new x-axis. The final x", y", and z" axes represent movement in the dip, strike, and dilation orientations of the fault. All measurement points, both axis systems, and the left and right fault blocks are identified in Figure 3.

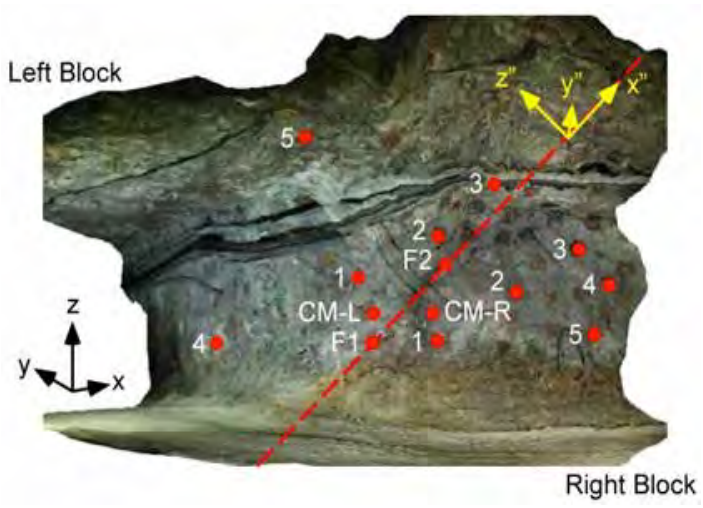

Figure 3. Illustration of measuring points (red dots), global axis system (lower-left in black), local axis system (upper-right in yellow) and left and right fault blocks at the 5600 Sublevel site. The thrust, slip, and convergence vectors of the fault are represented by x", y", and z", respectively.

Another potential use for photogrammetric methods can be seen by this analysis. Photogrammetric measurements of global displacements are compared to local displacements at the 5600 Sublevel site. Though crackmeter measurements indicated significant movement near the fault, they provided little information in terms of overall movement. Photogrammetric data indicated movement of both fault blocks in both the dip-slip (+ x") and the strike-slip vectors (+ y"). The latter of these two photogrammetric observations seems to confirm mine personnel observations of rib convergence. Additionally, there appeared to be a slight separation of the right block from the left block in the dilation orientation (z"). This also confirms observations of skin deterioration, and the consequent apparent widening of the fault exposure. Overall, the primary rock mass movement appears to be rib convergence, with the apparent fault movement more likely being a result of movement in the skin of the excavation, rather than global fault offset.

• *Case study 2 – 5700A Sublevel*

An additional photogrammetric case study was completed for the 5700A Sublevel of the same mine. The crackmeter at this site also measured significant movement, though on a much smaller scale than the previously examined 5600 site. Furthermore, overall ground conditions at the 5700A site were much better than the 5600 site during the period of photogrammetric and crackmeter monitoring. This case study was completed to determine how photogrammetry could track fault behavior, and thus, how it may supplement crackmeter instrumentation at a site not undergoing severe creep and rib closure.

Actual crackmeter measurements from the 5700A site indicated 6.2 mm of crackmeter extension between October 2013 and January 2015. Photogrammetry-produced, or virtual crackmeter measurements indicated 6.4 mm of extension during the same period. Unlike the previous case, point cloud comparisons did not show large scale rib deformation. That is, it appeared that movement was largely limited to fault offset. Crackmeter interpretation indicated that the hangingwall was moving downwards relative to the footwall.

A point movement analysis was conducted to determine the amount and type of fault offset at the 5700A site. The global coordinates of each crackmeter anchor, along with five additional points on each block, were converted to local coordinates using the fault's strike and dip (N 63º E and 58º, respectively). The collective movements of the points on each block were averaged to identify trends in fault block behavior. A trend was identified that corresponded to crackmeter interpretation shown in Figure 2, Scenario A. The average hangingwall movement in the dip shear orientation (x") is negative, indicating that the crackmeter should have measured elongation. Relative strike shear movement (y") of both fault blocks indicates uniform creep, thus likely not being the result of fault movement. Finally, average movement in the dilation orientation (z") indicated little in terms of opening or closing of the fault.

• *Case study conclusions*

Crackmeters can provide highly accurate local measurements in real time. Several crackmeters may also be used together to gain a sense of global movement trends. The primary hindrance to practical implementation of these photogrammetric techniques is long data processing and interpretation times. Once photogrammetric data is interpreted, however, full-field deformations can be quantified. As seen in the 5600 Sublevel case study, crackmeter data provided limited understanding of overall movement. While the crackmeter at this site did register significant movement, it missed rib movement throughout the site. Photogrammetric data, on the other hand, measured large-scale deformation at the 5600 Sublevel, and data from the 5700A Sublevel case study indicated specifically which fault block was moving. However, in both case studies, photogrammetric analyses were time-consuming, delaying insight into ground movement. They also could not discern how movement occurred in time. One of the full benefits of photogrammetry may be most apparent in volumetric monitoring as opposed to point-movement monitoring.

Volume Calculation

• *High energy, high deformation testing*

A third application of photogrammetry by NIOSH/SMRD researchers involves correlating volume of deformation with energy release. Ground control safety often depends on supporting, or at least containing, the ground between the rockbolts. Shotcrete and mesh, in various combinations and with other components, are often used to do this. A test method dubbed High-Energy High-Displacement

(HEHD) was developed to investigate this type of deformation (Martin, et al., 2015).

Photogrammetric observation of HEHD panel testing was conducted to track volume changes of a specimen as it is point loaded. This information could then be used to delineate the relationship between volume change due to deformation and remaining capacity of the support system. This can be done by correlating volumetric displacements of shotcrete panels with known displacements and loads obtained during panel tests. This technique may also be applied to mesh or reinforced shotcrete installed in a mine to infer remaining support toughness from observed volumetric changes. This is particularly important knowledge where seismic loading may impart significant energy to the support system. Thus, photogrammetric methods can aid in designing a safe work site.

• *Volume-energy relationship analysis*

To conduct the photogrammetric analysis, photographic image pairs were selected at 5 cm displacement intervals of the loading ram. These pairs were reconstructed in 3D for volumetric analysis. Volume-energy relationship analyses were conducted for three types of shotcrete panels. A weakest-to-strongest spectrum for analysis was created by using a panel made of a standard shotcrete mix (no reinforcement), a panel made of poly-fiber shotcrete mix (fiber reinforced), and a panel made with cyclone fencing enclosed in a fiber shotcrete mix (mesh and fiber reinforced). Additional tests using only 1.8x1.8 m sections of cyclone fence and welded wire mesh with no shotcrete were conducted as baselines. Synchronized clock times were established prior to each test between the cameras and data logger. The load and displacement data for each test were used to calculate energy, which was then matched with digitally recorded time stamps for each photograph pair. These data were used to match photogrammetric data with the calculated energy data at the 5 cm ram displacement intervals. Corresponding volume changes acquired through photogrammetric measurement were then compared to energy calculations for each interval.

Panel volumes remained relatively constant for each interval, regardless of panel type. This was expected because both dimensional measurements were based on similar ram displacements. The slight variability in volume and height were due to panel surface texture and geometry of panel failure. More significant, however, is the relationship between volume change and energy input. Figure 4 (top) shows volume-energy relationship. The effect of shotcrete reinforcement is clear in terms of energy absorption capacity. Cyclone-reinforced fiber shotcrete can withstand energies over 400% greater than standard mix shotcrete while undergoing the same volume of deformation. A clear difference in performance between the three types of shotcrete can be identified from this analysis. Assuming 1.3x1.3 m bolt spacing, the potential exists for a yield "volume" to be assessed in field settings. While standard and fiber mix shotcretes appear to lose load-bearing capacity at deformation volumes of 0.10 m^3, cyclone-reinforced fiber shotcrete can still assume more loading even at deformation volumes of 0.25 m^3. At present it is not possible to determine whether the better performance of cyclone-reinforced fiber shotcrete is the result of fencing reinforcement, or the fiber in combination with the fencing. Future tests of cyclone-reinforced standard mix shotcrete panels still need to be conducted.

The cyclone fence test provided less conclusive results. It required approximately 9 cm of ram displacement before the fencing started to provide significant resistance. This is because the fencing is relatively loosely constructed and that there is play in the system until the links make contact/interlock and start to develop tension in the steel strands. The force then begins to increase linearly with further displacement as the chain link fence begins to tighten and the wire strands are loaded in tension within their elastic region. With enough displacement, the chain link fence would be expected to exhibit ductile deformation. The welded wire mesh tests provided slightly better results, requiring less displacement (3 cm) before reaction began. However, no point of failure was reached, because of the same factors that limited the cyclone fence testing. Without

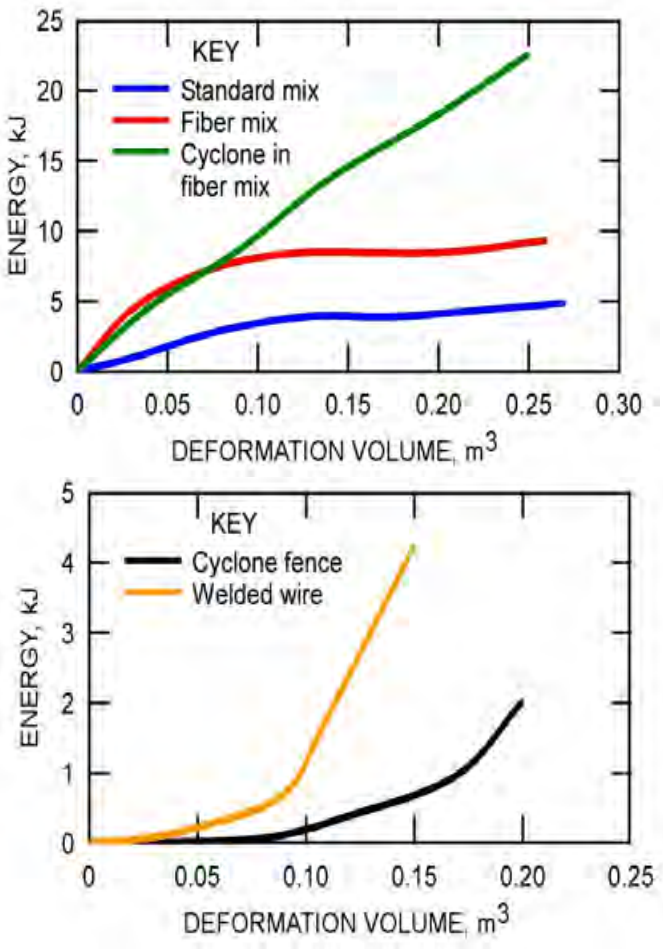

Figure 4. Relationship between energy and volume for shotcrete support systems (top), and wire mesh types (bottom), as determined through photogrammetric measurement.

shotcrete, both types of mesh have, on their own, essentially no load carrying capacity until excessive deformations occur. Since the test stopped at 25 cm of displacement, behavior of the cyclone fencing and welded wire mesh at failure was not observed. The energy-volume relationship for each type of mesh can be seen in Figure 4 (bottom).

• *Field volume measurements*

Researchers used specific in-mine reconstructions to correlate laboratory volume measurements to field volume measurements. The numerical methods used to determine laboratory testing volumes were used to calculate field deformation volumes. Site selection was based on two factors: range of deformation at the site, and orientation of jointing. The chosen site displayed varying levels of deformation, ranging from minor (< 3 cm) to severe (> 30 cm). Areas of the rib with roughly 1.8x1.8 m sides were chosen for both minor and severe cases of deformation, as well as an additional area of significant (~ 15 cm) deformation. Bedding at the site was parallel to the rib face, an orientation that leads to greater deformation.

Following techniques used in laboratory volume measurements, each 1.8x1.8 m area of the field site was considered as a uniform "panel" securely pinned by bolts at its corners. The volume of "bagged" or "bulged" material within the perimeter of bolts was treated as the bulge deformation of the shotcrete panels. It should be made clear, however, that cyclone fencing only, and not shotcrete, was used for surface control at this particular field site. Agisoft® PhotoScan Professional Edition was used for field volume calculations (Agisoft, 2014). This software is more amenable to field calculations because before-and-after reconstructions are not needed to calculate volumes. Surfaces of bulging material can be isolated, trimmed, and transformed into stand-alone solids by bridging low points along the perimeter across the area. Side views of each area are shown in Figure 5. Area 1 was composed of loose slabs being pushed out between bolts, while Area 2 was primarily highly fractured material bagging in the mesh between the bolts. Conversely, Area 3 consisted of competent rock, with minimal extrusion between bolts.

Energy estimations were calculated by interpolating the data obtained from laboratory testing of cyclone mesh. Due to the obscured data for displacements less than 9 cm, the energy for Area 3 could only be estimated as less than 100 J. Areas 1 and 2, however, could be assessed as having undergone approximately 3000 J and 8900 J of work, respectively. Confidence in the accuracy of the calculated volumes is based on their apparent correlation with volumes calculations derived from laboratory testing of panels having similar 1.8x1.8 m surface areas. Refinement of field volume calculations would include calibration and optimization of Agisoft's PhotoScan software in both laboratory and field settings. Further applications of these techniques include usage at shotcrete reinforced sites, and calculations of volume loss in areas of keyblocking. At present, photogrammetric calculations of deformation volumes appears to be a viable technique for understanding rock mass behavior.

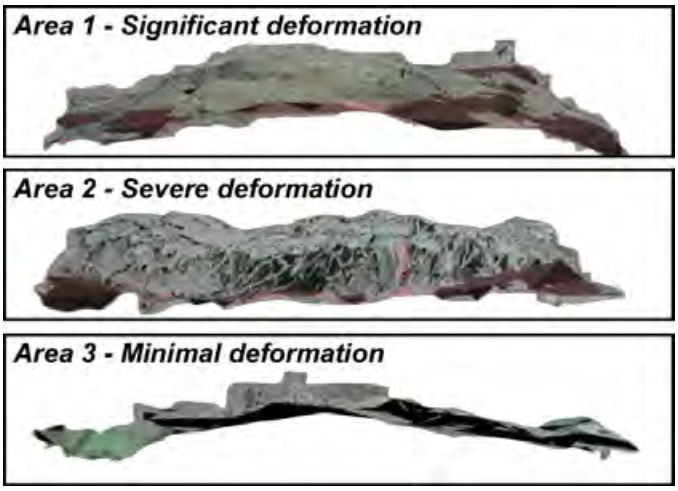

Figure 5. Side views of deformation areas selected for field deformation volume calculations. The Areas 1, 2, and 3 correspond to slabbing, fractured, and competent rock masses, respectively.

Conclusions

Photogrammetry was employed by NIOSH/SMRD researchers to monitor true ramp rib and back deformations at a deep underground mine. A catalog of geometric snapshots of ramp conditions over a period of two years was developed and implemented in a mine visualization project. These photogrammetric data may eventually become integrated with other recorded data, such as seismic event locations and stress instrumentation data.

Fault monitoring at the same mine has been conducted using photogrammetry, the results of which have been used to supplement crackmeter data. In two case studies, photogrammetry was found to confirm mine personnel observations of conditions, as well as inform crackmeter interpretation. At one site, severe rib deformation was found to override crackmeter readings of fault movement. At a second site, fault movement indicated by crackmeter elongation was supported by photogrammetric observation. In both cases, photogrammetry showed significant potential to supplement crackmeter monitoring techniques.

Lastly, laboratory photogrammetry was successfully implemented in shotcrete panel and mesh support system testing to delineate the relationship between bulge deformation and remaining strength. Results showed that significant differences in energy-absorbing capacity after deformation can be ascertained volumetrically for varying types of support. The results also indicate that yield volumes can be assessed in field settings. Field volume calculations show the same potential to estimate energy release based on amount of bulge deformation between bolts. These photogrammetric tech-

niques have potential to greatly increase the ability to assess field support conditions and requirements, and thus improve safety.

Acknowledgements

The authors gratefully acknowledge 3GSM and AdamTech for their guidance and cooperation in this research. Cooperating industry entities who allowed access and assistance in field research are also gratefully acknowledged. The work described in this paper would not have been possible without their time and expertise. The authors also acknowledge those who participated in the development of the HEHD testing system and construction of the shotcrete panels. Special thanks to the following NIOSH personnel: Lewis Martin, Jeffrey Johnson, Curtis Clark, Michael Stepan, Seth Finley, Mark Powers, Habte Abraham, Marc Loken, and Tex Kubacki for their laboratory assistance, Heather Lawson for her help in the field, Kenneth Strunk for his help with graphics, and Jeffrey Whyatt and Michael Jenkins for their assistance in editing and reviewing a preliminary version of this manuscript.

References

Agisoft LLC (2014). *Agisoft PhotoScan User Manual: Professional Edition, Version 1.1* available at http://www.agisoft.com/pdf/photoscan-pro_1_1_en.pdf.

Benton, D., Iverson, S., Johnson, J., and Martin, L. (2014). Photogrammetric Monitoring of Rock Mass Behavior in Deep Vein Mining. *Proceedings of the 33rd International Conference on Ground Control in Mining*, Morgantown, WV: West Virginia University, 221-227.

Benton, D., Iverson, S., Martin, L., Johnson, J., and Raffaldi, M. (2015). Volumetric Measurement of Rock Movement Using Photogrammetry. *Proceedings of the 34th International Conference on Ground Control in Mining*, Morgantown, WV: West Virginia University. Paper submitted for publication.

Board, M. (2015). Email correspondence regarding mine conditions, 04-03-2015.

Martin, L., Clark, C., Johnson, J., and Stepan, M., (2015). "A New High Force and Displacement Shotcrete Test." *Mining & Exploration Technology: Technology Development and Implementation in Rock Mechanics and Ground Control*, SME Annual Meeting, Feb. 15-18, 2015, Denver, CO: Preprint 15-090, 10.

Orr, T.J., MacDonald, B.D., Iverson, S.R., and Hammond, W.R. (2015). Development of a Generic Mine Visualization Tool Using Unity. F-2015-055. To be presented at the 37th International Symposium on the Application of Computers and Operations Research in the Mineral Industry, Fairbanks, AK, May 23–27.

Unity Technologies (2015). Unity Manual. Accessed at http://docs.unity3d.com/Manual/index.html